Development of 3D chromatin texture analysis using confocal laser scanning microscopy [1]

André Huisman [a], Lennert S. Ploeger [a], Hub F.J. Dullens [a], Neal Poulin [a], William E. Grizzle [b] and Paul J. van Diest [a,*]

[a] *Department of Pathology, University Medical Center Utrecht, Utrecht, The Netherlands*
[b] *Department of Pathology, University of Alabama at Birmingham, Birmingham, AL, USA*

Abstract. *Introduction*: Analysis of nuclear texture features as a measure of nuclear chromatin changes has been proven to be useful when measured on thin (5–6 μm) tissue sections using conventional 2D bright field microscopy. The drawback of this approach is that most nuclei are not intact because of those thin sections. Confocal laser scanning microscopy (CLSM) allows measurements of texture in 3D reconstructed nuclei. The aim of this study was to develop 3D texture features that quantitatively describe changes in chromatin architecture associated with malignancy using CLSM images. *Methods*: Thirty-five features thoughtfully chosen from 4 categories of 3D texture features (discrete texture features, Markovian features, fractal features, grey value distribution features) were selected and tested for invariance properties (rotation and scaling) using artificial images with a known grey value distribution. The discriminative power of the 3D texture features was tested on artificially constructed benign and malignant 3D nuclei with increasing nucleolar size and advancing chromatin margination towards the periphery of the nucleus. As a clinical proof of principle, the discriminative power of the texture features was assessed on 10 benign and 10 malignant human prostate nuclei, evaluating also whether there was more texture information in 3D whole nuclei compared to a single 2D plane from the middle of the nucleus. *Results*: All texture features showed the expected invariance properties. Almost all features were sensitive to variations in the nucleolar size and to the degree of margination of chromatin. Fourteen texture features from different categories had high discriminative power for separating the benign and malignant nuclei. The discrete texture features performed less than expected. There was more information on nuclear texture in 3D than in 2D. *Conclusion*: A set of 35 3D nuclear texture features was used successfully to assess nuclear chromatin patterns in 3D images obtained by confocal laser scanning microscopy, and as a proof of principle we showed that these features may be clinically useful for analysis of prostate neoplasia.

Keywords: Confocal laser scanning microscopy, 3D, texture features, image analysis, prostate cancer, nuclear chromatin

1. Introduction

The transformation of a normal cell into a malignant cell is associated with genetic alterations that result in morphological changes in the nucleus [24]. Those genetic changes can be assessed by molecular screening techniques on a global level (DNA Ploidy [3], patterns of chromosomal gains and losses [17]) or on a high resolution level (PCR, sequence analysis). For diagnostic purposes it is conventional and less cumbersome to assess the morphological implications of these genetic changes such as nuclear [10] or nucleolar size [20] or chromatin distribution [8,22]. The nuclear chromatin distribution in genetically altered cells is generally coarsely-clumped with multiple chromocenters and larger nucleoli in contrast to normal cells which characteristically have finely granular chromatin with few chromocenters and no or small nucleoli. These changes are often rather subtle or even subvisible, and are sometimes referred to as "malignancy associated changes" as they may be detected in morphologically benign cells when malignancy is present [13]. Therefore, they should better be quantified by "texture features" because they are very sensitive, even for small
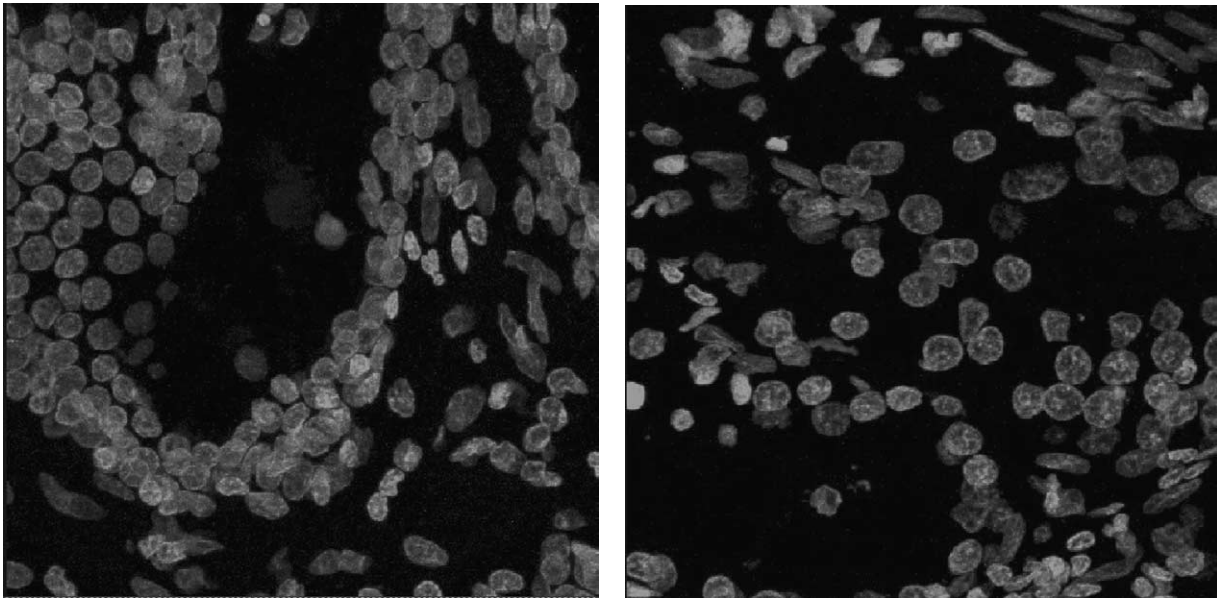
Fig. 1. The transformation of a normal prostate cell nucleus (left) into a malignant cell nucleus (right) is associated with nuclear chromatin changes. For example, the presence of large nucleoli, visible as relatively bright dots in the cell nuclei, are clearly visible in this example. These images are maximum intensity projections from the same confocal image stack.

textural changes, and are not prone to observer subjectivity. Figure 1 shows representative benign and malignant confocal planes illustrating these changes.

There is a vast amount of literature on the clinical value of the assessment of such texture features by image analysis in conventional tissue sections or cytospins prepared from cell suspensions, ranging from diagnostic [13] to prognostic applications [18]. Conventional thin tissue sections have the drawback that only a slice of the nucleus is present within the section, resulting in potential loss of important information. This can be avoided by preparing cytospins from cell suspensions, but this introduces artifacts by the flattening of nuclei while spinning them down at high speed, and the morphological context of the analyzed nuclei is completely lost by the dissociation process and by drying. These drawbacks can be avoided completely by using confocal laser scanning microscopy (CLSM) for imaging of nuclei in thick sections. Thin optical slices are taken at high resolution by confocal imaging, and these are subsequently reconstructed in 3D [14,19]. In spite of these major potential advantages, so far implementation of only a small number of 3D texture features was described in a single study [1]. In the present study we addressed this technical challenge and developed software for calculating 35 3D nuclear texture features. These were thought-

fully chosen from four categories of texture features: descriptive statistics for the grey-value distribution [6,15], features discriminating nuclear regions with a low, a medium and a high amount of DNA, Markovian features, derived from co-occurrence matrices [5,9] and fractal features [7]. This selection was based on their reported clinical usefulness when measured by conventional 2D image cytometry, their wide popularity for texture characterization, and their potential power to detect nucleoli. To be most advantageous in practice, such texture features need to have invariant properties with regard to rotation and scaling that make it possible to image cells under arbitrary orientations and using different zoom factors, which we thoroughly tested in artificially created images.

2. Methods

2.1. Implementation of 3D texture features

Measurement of the 35 selected texture features was done with the open source Image Processing ToolKit (ITK, Kitware Inc., New York, USA). Using this image processing library we computed the Markovian texture features. The other texture features were implemented in-house. We added a visualization module for 3D vol-

ume rendering, using the Visualization ToolKit (VTK, Kitware Inc., New York). In the appendix the formulas are listed.

2.2. Descriptive statistical features

These features summarize general statistics for the chromatin distribution [6]:

1. The Integrated Fluorescence Intensity (*IFI*) is comparable to the integrated optical density in conventional bright field microscopy. It is defined as the sum of grey-values of a nucleus, assuming no background noise. Due to the stoichiometry of the applied fluorescent stains this sum is proportional to the amount of DNA. This feature is theoretically rotation invariant, but not scale invariant.

2. In a straightforward way the Mean Fluorescence Intensity (*MFI*) can be defined, using *IFI* and the volume in voxels. This feature is theoretically scale and rotation invariant.

3. Variance of fluorescence intensity over the nucleus (2nd moment of the intensity distribution around the mean intensity) abbreviated as *FIVAR*. If the chromatin is distributed uniformly it is equal to 0. This feature is theoretically rotation and scale invariant. The standard deviation, *FISD*, is given by $\sqrt{FIVAR}$.

4. The asymmetry of the intensity distribution, the skewness (*FISKEW*) [15]. This feature is also theoretically rotation and scale invariant. For a normal distribution, the skewness is equal to 0.

5. Kurtosis: a measure for how far the tail-ends of the *IFI* distribution extend (this is equal to 0 for a Gaussian distribution) [15]. This feature is theoretically scale and rotation invariant.

2.3. Discrete texture features [6]

It is often possible to visually discern areas in the nucleus with different chromatin condensation states, corresponding to different ranges of grey-values. We define the low density area as the area containing pixels with a grey-value in the range from [0, *MFI* − *FISD*], the medium density area with grey-values in the range (*MFI* − *FISD*, *MFI* + *FISD*] and the high density area with grey-values in the range (*MFI*+*FISD*, ∞). For nuclei with normally distributed grey values the relative number of pixels is respectively 16%, 68% and 16%. Those numbers were used to validate the segmented

sizes of the condensation state areas. We segmented the nuclei in those regions and computed the following texture features.

1. The volume of the regions with low (*VOLUME$_L$*), medium (*VOLUME$_M$*) or high (*VOLUME$_H$*) amount of DNA in μm^3, estimated by multiplying the voxel dimensions for every dimension and the number of object pixels. This feature is theoretically rotation but not scale invariant.

2. The number of different objects per condensation state A, i.e. the number of separated regions for a certain state. This feature is theoretically rotation and scale invariant.

3. The relative amount of DNA in a region A, called extinction ratio. This feature is theoretically rotation, but not scale, invariant.

4. Comparison of ratios between the mean intensity of the low condensation state and the respective other condensation states A, called average extinction ratio (*AVG_EXTINCTION*). Higher feature values for all those average extinction ratios indicate smoother transitions between chromatin condensation states. This feature is theoretically invariant under scaling and rotation.

5. The compactness of the surfaces of the different condensation states is used as a measure for the circularity. The surface of the enclosing surfaces is computed for all objects in the condensation state. In our implementation, the surfaces were computed by triangulation of the condensation states and integrating the area of the triangles. The value of compactness equals 1 for a sphere. This feature is theoretically rotation, but not scale invariant.

6. The average distance between the geometrical centre of the nucleus and all voxels from each chromatin state. This indicates how close the chromatin is located to the border. The function $d(C, (i, j, k))$ is defined as the Euclidean distance between the geometrical center of the nucleus, C, and the coordinate (i, j, k). It is normalized with the volume of the chromatin state (*VOLUME$_A$*) and the average radius of the nucleus (R). The average distance is 1 if all voxels from a certain condensation state are on the nuclear border (i.e. as far from the center of the nucleus as possible). This feature is theoretically rotation and scale invariant.

7. The distance between the geometrical centre of the nucleus (C) and the center of mass of each chromatin condensation state (*CM$_A$*). It is nor-

malized with the volume of the chromatin state ($VOLUME_A$) and the average radius R of the nucleus. The value of this feature is zero if the chromatin states are distributed symmetrically with respect to the nuclear center. This feature is theoretically rotation and scale invariant.

2.4. Markovian texture features

Markovian texture features describe texture patterns more locally and are typically computed from a co-occurrence matrix [9]. They characterize the second order gray-level distribution of an image. The elements of the co-occurrence matrix describe the joint probability that a gray-level i co-occurs with a gray-level j on a distance d under angle θ and inclination ϕ. Texture features are derived from the co-occurrence matrix. The features we calculated are: Energy, Entropy, Correlation, Difference Moment, Inertia, Cluster Shade and Cluster Prominence [9]. These features are fundamentally not rotation and scale invariant. However, rotation invariance is achieved by computing co-occurrence matrices for different angles and inclinations and combining those matrices by averaging. Scale invariance could be introduced by using multi-resolution techniques (e.g. image pyramids). However, since our aim was to compare cell nuclei at the same scale, we did not correct these features for scale variance.

2.5. Fractal texture features

Fractals are mathematical objects which have similar details on different scales. The advantage of fractals is that their complexity is invariant under scaling and have a strong correlation with human judgment of roughness of texture [4]. In our software implementation we used the box-counting approach [16].

The fractal dimension is a feature used to characterize the geometrical complexity of the chromatin pattern. However, two different objects can have the same fractal dimension. Therefore another feature is needed to characterize the fractal more precisely. One such feature is the lacunarity, which characterizes the size of gaps or holes of a fractal, in this particular context chromatin clearings and nucleoli. The calculation of the lacunarity was implemented using a gliding box approach [7].

3. Verification of implementation using model images

We verified our software implementation using images of artificially generated ovoid 3D objects simulating nuclei, for which the true values for texture feature values are mathematically defined. These images were defined as having an isotropic resolution. For the discrete and general statistical features, these objects were generated with Gaussian distributed grey-values (mean and standard deviation of 740.0 and 400.0).

For the discrete texture features, we verified the intra-nuclear segmentation by assessing the areas of the low, medium and high condensation states. These areas were respectively 16%, 68% and 16% as expected. The ITK software provided the algorithms to validate the Markovian features. This was done by manually defining grey values within an artificial image, computing the Markovian texture feature values with the implemented algorithms, and comparing these to reference values. The computation of the fractal dimension was verified using the above described artificial nuclei. The fractal dimension is known to be 2 for normally distributed images [11]. The lacunarity computation was verified using artificial 3D nuclei having uniformly distributed grey-values, the number of lacunas being known from the distribution parameters.

The procedure was repeated for the same object under an angle of 90° and a magnification factor of 8 to test for rotation and scale invariance, respectively.

Table 2 shows AUC values for features discriminating benign and malignant artificial nuclei with different degrees of chromatin margination and nucleolar sizes. Most features were both sensitive for nucleolar size and chromatin margination. Features that remained discriminative although the effect of the nucleolar size and chromatin margination was very limited are marked with a plus sign. Features that were never able to discriminate between the benign and malignant artificial nuclei were *Inertia* and *Correlation*, both derived from the co-occurrence matrix, the *Volume of the low and high condensation states,* the *Compactness of the medium and high condensation states*, and the *Fractal dimension*.

4. Assessment of clinical value by discriminating benign and malignant model and prostate nuclei

The discriminative power of our features was tested on the above described artificially generated ovoid

shaped nuclei with normally distributed grey-values that were used as a model of benign nuclei. These nuclei were compared with artificial malignant nuclei, which were modeled to have normally distributed grey-values with the same parameters as the benign nuclei, but with an added nucleolus and the DNA located more towards the border. The grey-value of the nucleolus was set to 3276, 80% of the maximum grey-value for a 12 bit signal-depth. The ovoid shaped area containing a low amount of DNA was centered in the nucleus. This region has normally distributed grey values, with a mean value of 370 and a standard deviation of 200. These nuclei were constructed to fit in a bounding box with dimensions of $80 \times 80 \times 12$ voxels. Figure 2 shows examples of these artificial nuclei. The size of the ovoid shaped nucleolus was varied, together with the radius of a central nuclear region with a relatively low amount of DNA to simulate chromatin margination. By varying these radii we established the sensitivity of the 3D texture features.

For further clinical validation, a fourteen micron thick section from a prostatectomy specimen containing prostate cancer was stained with TO-PRO-3 (Molecular Probes, Eugene, OR, USA) and subsequently imaged in 3D in a semi-automated fashion by confocal laser scanning microscopy (Leica TCS SP2 AOBS, Leica Microsystems, Heidelberg, Germany). Segmentation of the cell nuclei was performed by our previously developed software for 3D segmentation of cell nuclei images acquired with CLSM [2]. The segmentation results were exported to our texture feature computation software for feature calculation of benign and malignant cells as judged by a pathologist (PvD). The parameters of the normal distribution of the artificially cre-

ated cell nuclei (mean of 740 and standard deviation of 400) were established from the mean and variance of these benign nuclei.

In univariate analysis, Receiver Operating Characteristic (ROC) analysis was used to discriminate between benign and malignant model nuclei [23], varying the radius of the size of the central area with a low amount of DNA and the size of the nucleolus. The area under the ROC curve (AUC) was used as a measure for the discriminative performance (0.5–1) of an individual feature [21].

5. Discriminating benign and malignant prostate nuclei: 2D vs 3D

In order to assess the added value of using the complete 3D image stack in nuclear texture feature calculations compared to bright-field microscopy, we re-implemented the 3D texture features for 2D application. Using the 3D stacks of the 10 benign and 10 malignant prostate nuclei as described above, we identified the central plane for each nucleus, calculated the 35 textures features in this single plane, and compared the AUC values between these 2D features with the 3D features calculated for the whole nuclei.

6. Results

Table 1 shows the theoretical and experimentally established invariance properties of the implemented texture features. All features showed the theoretically expected invariant properties. From the descriptive sta-
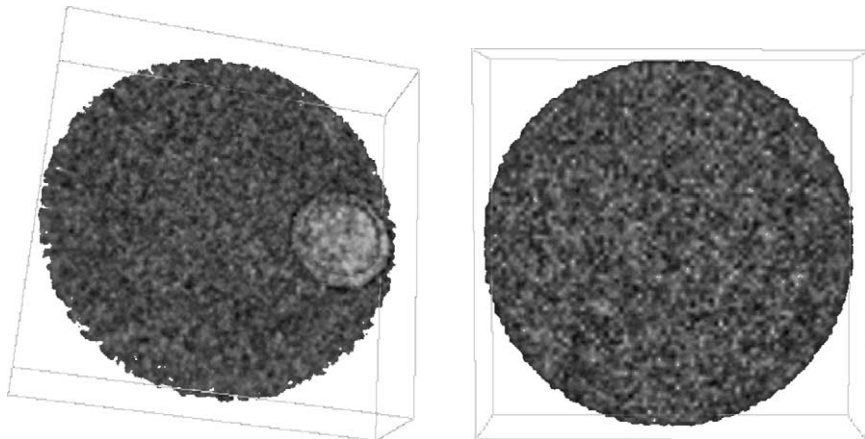

Fig. 2. Volume rendering of artificial 3D nuclei used to test 3D nuclear texture features. Left: image representing benign nucleus with normally distributed grey values and no nucleolus. Right: image representing malignant nucleus with the margination of the chromatin and a nucleolus.

Table 1

Invariance properties of 35 implemented 3D texture features computed on artificial nuclei having a nuclear size of 10 μm and a nucleolar size of 3 μm and a scaling of the central area with a low amount of DNA of 0.5 with respect to the nuclear size. The percentages are relative changes with respect to the initial image from which the rotated and scaled images were computed

Texture feature	Rotation invariance		Scale invariance	
	Theoretical	Practical	Theoretical	Practical
Descriptive statistical features				
Integrated fluorescence intensity	Yes	0.00%	No	700%
Mean fluorescence intensity	Yes	0.00%	Yes	0.00%
Fluorescence intensity variance	Yes	0.00%	Yes	0.00%
Skewness of the fluorescence intensity distribution	Yes	0.00%	Yes	0.00%
Discrete texture features				
Kurtosis of the fluorescence intensity distribution	Yes	0.00%	Yes	−0.01%
Volume	Yes	0.00%	No	700%
Average extinction ratio	Yes	0.00%	Yes	0.00%
Relative extinction ratio compared to low condensation state	Yes	0.00%	Yes	0.00%
Number of not connected objects per condensation state	Yes	0.00%	Yes	0.00%
Compactness	Yes	0.03%	Yes	1.22%
Markovian texture features				
Average distance between geometrical nuclear center and all pixels in a condensation state	Yes	0.00%	No	9.99%
Normalized asymmetry of condensation states through the nucleus	Yes	0.00%	No	2.44%
Energy	Yes	0.00%	No	$1.17 \cdot 10^3$%
Entropy	Yes	0.00%	No	43.1%
Correlation	Yes	0.00%	No	5.85%
Difference moment	Yes	0.00%	No	$1.15 \cdot 10^3$%
Fractal texture features				
Inertia	Yes	0.00%	No	27.4%
Cluster shade	Yes	0.00%	No	82.0%
Cluster prominence	Yes	0.00%	No	−77.8%
Lacunarity	Yes	0.00%	No	85.1%
Fractal dimension	Yes	0.00%	Yes	1.15%

tistical features, as expected *IFI* was not scale invariant. Also as expected, from the six discrete texture features, *Volume*, the *average distance between the geometrical nuclear center and all pixels of a condensation state* and the *Normalized asymmetry of the condensation states throughout the nucleus* were clearly not scale invariant as expected. None of the Markovian texture features were scale invariant. From the fractal texture features, the fractal dimension was scale invariant as expected. The results on the artificial nuclei with known grey-value distributions and image properties were as predicted. Together with the invariant results, this indicates that a correct software implementation was achieved. The apparent rotation variance of the compactness feature is due to several estimation and rounding errors during the computation of this feature.

Table 3 shows the computed AUC values for the different texture features as measures for their discriminative power between the 10 benign and 10 malignant prostate nuclei. The following features had AUC values of 0.80 or greater: the *Number of unconnected parts of the low condensation state, Low versus medium-high average extinction ratio, Low versus high average extinction ratio, Cluster prominence, Entropy, Grey variance, Energy, Correlation, Grey mean, Inertia, Grey kurtosis, Inverse difference moment* and *Average extinction ratio of region with low amount of DNA*.

In the 2D/3D comparison, the AUC values of the 20 best discriminating features, computed in 3D, were significantly higher ($p = 0.001$, Wilcoxon signed ranks test) when computed for 3D whole nuclei than when assessed in the single central 2D plane.

Table 2

Discriminative power for artificial 3-D nuclei with varying nucleolar size and degree of chromatin margination of 3D nuclear texture features yielding an area under the curve in ROC analysis of 0.5 and higher. Texture features marked with a plus sign indicate a low sensitivity to the effects of these variations

Nucleolar size	0		0.03			0.06			0.09			0.1		0.2	0.3		0.4	0.4			0.5			0.6		Total
Chromatin margination	0.1	0.2	0	0.1	0.2	0	0.1	0.2	0	0.1	0.2	0.5	0.9	0.5	0.5	0.9	0.5	0.7	0.9	0.9	0.5	0.7	0.9	0.5	0.9	
Grey sum	0	0	1	0	0	1	1	0	1	1	0	0	0	0	1	0	1	1	1	0	1	1	1	1	1	14
Grey mean	0	0	1	0	0	1	1	0	1	1	0	0	0	0	1	0	1	1	1	0	1	1	1	1	1	14
Grey variance	0	0	1	1	1	1	1	1	1	1	1	1	0	1	1	1	1	1	1	1	1	1	1	1	1	22
Grey skewness +	1	1	1	1	1	1	1	1	1	1	1	1	1	1	1	1	1	1	1	1	1	1	1	1	1	25
Grey kurtosis +	1	1	1	1	1	1	1	1	1	1	1	1	1	1	1	1	1	1	1	1	1	1	1	1	1	25
Energy +	1	1	1	1	1	1	1	1	1	1	1	1	1	1	1	1	1	1	1	1	1	1	1	1	1	25
Entropy +	1	1	1	1	1	1	1	1	1	1	1	1	1	1	1	1	1	1	1	1	1	1	1	1	1	25
Inverse difference moment +	1	1	1	1	1	1	1	1	1	1	1	1	1	1	1	1	1	1	1	1	1	1	1	1	1	25
Cluster shade	1	1	0	0	0	1	1	1	0	0	0	1	1	1	1	1	1	1	1	1	1	1	1	1	1	19
Cluster prominence	1	1	0	0	0	0	0	0	0	0	0	0	0	1	1	1	1	1	1	1	1	1	1	1	1	14
Volume of medium region	1	0	1	1	1	1	1	1	1	1	1	1	1	1	1	1	1	1	0	1	1	1	0	1	0	21
Average extinction ratio of low region	0	1	0	0	0	0	0	0	0	0	0	0	0	0	0	0	0	0	1	0	0	0	1	0	1	4
Average extinction ration of medium region	1	0	1	1	1	1	1	1	1	1	1	0	1	1	1	1	1	1	1	1	0	0	1	0	1	20
Average extinction ration of high region	0	1	0	0	0	0	0	0	0	0	0	1	0	0	0	0	0	0	1	1	1	1	1	1	1	9
Low vs. medium avg. ext. rat. +	1	0	1	1	1	1	1	1	1	1	1	1	1	1	1	1	1	1	1	1	1	1	1	1	1	24
Low vs. med-high avg. ext. rat. +	1	1	1	1	1	1	1	1	1	1	1	1	1	1	1	1	1	1	1	1	1	1	1	1	1	25
Low vs. high avg. ext. rat. +	1	1	1	1	1	1	1	1	1	1	1	1	1	1	1	1	1	1	1	1	1	1	1	1	1	25
Number of unconnected low areas	0	1	0.5	0	1	1	1	1	1	1	1	1	1	1	1	1	1	1	1	1	1	1	1	1	1	22.5
Number of unconnected high areas	1	0	0	0.5	0	1	1	1	1	1	1	0	1	1	1	1	1	1	1	1	0	0	1	0	1	17.5
Compactness of low region	0	0	0	0	0	0	0	0	0	0	0	1	1	1	1	1	1	1	0	1	1	1	0	1	0	11
Compactness of high region	0	1	0	0	0	0	0	0	0	0	0	0	1	0	1	0	0	0	0	0	0	0	0	0	0	3

Table 2
(Continued)

Nucleolar size	0		0.03			0.06			0.09			0.1		0.2	0.3		0.4	0.4			0.5			0.6		Total
Chromatin margination	0.1	0.2	0	0.1	0.2	0	0.1	0.2	0	0.1	0.2	0.5	0.9	0.5	0.5	0.9	0.5	0.7	0.9	0.9	0.5	0.7	0.9	0.5	0.9	
Average distance to geo-center from low region	0	0	0	0	0	0	0	0	0	0	0	0	0	0	0	0	0	0	1	1	1	0	1	1	1	6
Average distance to geo-center from medium region	1	1	0	1	1	0	0	0	0	0	1	0	0	0	0	0	1	0	1	0	1	1	1	1	1	12
Average distance to geo-center from high region	1	1	1	1	1	1	1	1	1	1	1	1	1	1	1	1	1	1	1	1	0	0	1	0	1	22
Asymmetry of distribution of low region through nucleus	0	0	0	0	1	0	0	1	0	0	0	1	1	1	1	1	1	1	1	1	1	1	1	1	1	16
Asymmetry of distribution of medium region through nucleus	0	0	0	0	1	1	0	1	0	1	0	0	1	1	1	1	1	1	1	1	1	1	1	1	1	17
Asymmetry of distribution of high region through nucleus	1	0	0	0	1	1	1	1	1	1	1	1	1	1	1	1	1	1	1	1	1	1	1	1	1	22
Lacunarity +	1	1	1	1	1	1	1	1	1	1	1	1	1	1	1	1	1	1	1	1	1	1	1	1	1	25
Total number of features	17	16	16	15	18	20	19	19	18	19	17	18	20	21	24	21	24	23	25	23	23	22	25	23	25	

Table 3

Discriminative power of 3D nuclear texture features for benign and malignant prostate nuclei imaged from a prostatectomy specimen in thick tissue sections by CLSM stained with TO-PRO-3. The texture features having an AUC of 0.80 or greater in ROC analysis are shown

3D Texture feature	AUC
Number of unconnected parts of low condensation state	0.80
Low versus medium-high average extinction ratio	0.87
Low versus high average extinction ratio	0.87
Cluster prominence	0.88
Entropy	0.91
Grey variance	0.92
Energy	0.94
Correlation	0.94
Grey mean	0.97
Inertia	0.98
Grey kurtosis	0.99
Inverse difference moment	0.99
Average extinction ratio of region with low amount of DNA	0.99
Grey skewness	1.00

7. Discussion

The aim of this study was to develop software approaches to analyze multiple 3D nuclear texture features in order to detect subtle changes in nuclear chromatin patterns in thick tissue sections imaged by confocal laser scanning microscopy. Thirty-five features were thoughtfully chosen from four categories of texture features. The software implementation of these features were tested for invariance with regard to rotation and scaling in model images. When the expected results were obtained illustrating correct implementation, the discriminative power of these features was tested on artificial 3D nuclei to establish whether the texture features were sensitive for nucleolar size and/or chromatin margination. It appeared that almost all features were sensitive to variations in the nucleolar size and for the degree of chromatin margination.

Their discriminative power to separate benign and malignant prostate nuclei was also tested. It appeared that 14 texture features were able to discriminate (AUC $\geqslant$ 0.80) the benign and malignant nuclei. From those features, 4 are from the category of discrete texture features, 4 are general grey-value statistics and 6 are from the category of Markovian texture features. From those 14 features, according to our model studies 9 were not sensitive to an increase in nucleolar size and degree of chromatin margination, 2 were not discriminative at all and 3 only for larger nucleoli and advanced chromatin margination. We expected the discrete features to perform well, because they correspond closely with the visual changes occurring during the development of malignancy in prostate cancer, namely the appearance of a prominent nucleolus and margination of the chromatin. However, the discriminative power of these features was less than expected, due to the number of regions and the thresholds used to define those regions. Markovian features are known to perform well in 2D [21] and we showed that they also perform well in 3D.

In order to assess the added value of the third dimension in nuclear texture feature calculations, we re-implemented the 3D texture features for 2D application. Using the 3D stacks of the 10 benign and 10 malignant prostate nuclei as described above, we identified the middle plane for each nucleus, calculated the 35 textures features in this single plane, and compared the AUC values between these 2D features with the 3D features calculated for the whole nuclei. The 20 best performing features had significantly better AUC values in 3D than in 2D, indicating that there is more nuclear texture information in 3D than in 2D. When comparing texture data from 2D images obtained from wide field microscopy to a 3D confocal image stack the difference in texture information will be even larger than in our experiment due to the larger depth of field of regular wide-field microscopy.

Although successful implementation of 3D texture features has now been achieved, some further improvements can be expected by implementing corrections for the scale variance of some of the features. Improvements are likely to be achieved when using new optical techniques, like 4pi microscopy, resulting in better images, or, more practically by the use of deconvolution algorithms [12] that deblur the images, resulting in more image information in the Z-direction. Such improvements in image quality will compensate for the potential rotational variance in texture feature calculation due to the relatively low amount of Z-information. Furthermore, the Markovian texture features will have more discriminative power, since they are computed by combining information from the Z-direction as well as in-plane information. These texture features are thus biased by the blurring in the Z-direction.

Now that we have implemented a large amount of 3D texture features, which has not been done previously at this scale, and the proof of principle demonstrates that these features may be clinically useful, a more extensive clinical evaluation will be completed. This will initially concern discriminating benign and malignant prostatic nuclei in prostatectomy specimens,

then biopsies, and will also involve detecting malignancy associated changes in morphologically benign nuclei from cancer cases as predictive markers and as surrogate endpoints for evaluating therapy, especially preventive interventions.

In conclusion, successful implementation has been achieved of 35 3D nuclear texture features. This technique can be used to detect the presence of nucleoli, among other textural changes and to assess nuclear chromatin patterns in 3D images obtained by confocal laser scanning microscopy. As a proof of principle we demonstrated that these features may be useful clinically for analysis of neoplastic changes in prostate tissue.

Appendix: Texture feature formulas

In the remainder, the following notation is used: $I(i, j, k)$ denotes the intensity at voxel (i, j, k), where i, j and k are discrete indices in the image. The coordinate (x, y, z) denotes a point in world-space. N is the number of voxels and *Volume* is nuclear volume.

A. *Descriptive statistical features* [6]

1. Integrated fluorescence intensity:

$$IFI = \sum_{i,j,k} I(i, j, k).$$

2. Mean fluorescence intensity:

$$MFI = \frac{IFI}{VOLUME}.$$

3. Fluorescence intensity variance:

$$FIVAR = \frac{\sum_{i,j,k}(I(i, j, k) - MFI)^2}{(N - 1)(MFI)^2}.$$

The standard deviation, *FISD*, is given by $\sqrt{FIVAR}$.

4. Skewness of the fluorescence intensity distribution [15]:

$$FISKEW = \frac{\sum_{i,j,k}(I(i, j, k) - MFI)^3}{N \cdot FISD^3}.$$

5. Kurtosis of the fluorescence intensity distribution [15]:

$$FIKUR = \frac{\sum_{i,j,k}(I(i, j, k) - MFI)^4}{N \cdot FISD^4} - 3.$$

B. *Discrete texture features* [6]. The subscript A is used to denote a specific chromatin condensation state. Texture features are computed for several different condensation states.

3. Extinction ratio:

$$amount(A) = \frac{IFI_A}{IFI}.$$

4. Average extinction ratio:

$$avg\_extinction(A) = \frac{MFI_A}{MFI_{\text{low}}}.$$

5. Compactness:

$$compactness = \frac{p_A^3}{36\pi VOLUME_A^2}.$$

6. Average distance to geometrical center. $d(C, (x, y, z))$ is defined as the Euclidean distance between the geometrical center C and coordinate (x, y, z):

$$average\_distance(A)$$
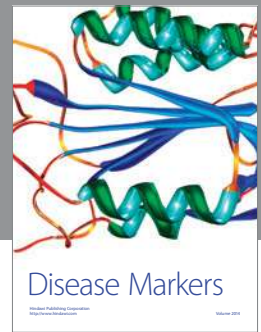$$= \frac{\sum_{x,y,z \in A} d(C, (x, y, z))}{VOLUME_A \overline{R}}.$$

7. Asymmetry. CM_A denotes the center of mass of condensation state A:

$$asymmetry(A) = \frac{d(CM_A C)}{VOLUME_A \overline{\overline{R}}}.$$

References

[1] M. Beil, T. Irinopoulou, J. Vassy et al., Chromatin texture analysis in 3-dimensional images from confocal scanning laser microscopy, *Analytical and Quantitative Cytology and Histology* **17** (1995), 323–331.

[2] J.A. Belien, A.H. van Ginkel, P. Tekola et al., Confocal DNA cytometry: a contour-based segmentation algorithm for automated three-dimensional image segmentation, *Cytometry* **49** (2002), 12–21.

[3] E. Bergers, J.P. Baak, P.J. van Diest et al., Prognostic value of DNA ploidy using flow cytometry in 1301 breast cancer patients: results of the prospective Multicenter Morphometric Mammary Carcinoma Project, *Mod. Pathol.* **10** (1997), 762–768.

[4] B.B. Chaudhuri and N. Sarkar, Texture segmentation using fractal dimension, *IEEE Transactions on Pattern Analysis and Machine Intelligence* **17** (2005), 72–77.

[5] A.E. Dawson, E.S. Cibas, J.W. Bacus et al., Chromatin texture measurement by Markovian analysis. Use of nuclear models to define and select texture features, *Analytical and Quantitative Cytology and Histology* **15** (1993), 227–235.

[6] A. Doudkine, C. Macaulay, N. Poulin et al., Nuclear texture measurements in image cytometry, *Pathologica* **87** (1995), 286–299.

[7] A.J. Einstein, H.S. Wu, M. Sanchez et al., Fractal characterization of chromatin appearance for diagnosis in breast cytology, *J. Pathol.* **185** (1998), 366–381.

[8] M. Guillaud, A. Doudkine, D. Garner et al., Malignancy associated changes in cervical smears: systematic changes in cytometric features with the grade of dysplasia, *Anal. Cell Pathol.* **9** (1995), 191–204.

[9] R. Haralick, K. Shanmugam et al., Textural features for image classification, *IEEE Transactions on Systems, Man and Cybernetics* **3** (1973), 610–620.

[10] I. Jannink, J.N. Bennen, J. Blaauw et al., At convenience and systematic random sampling: effects on the prognostic value of nuclear area assessments in breast cancer patients, *Breast Cancer Res. Treat.* **36** (1995), 55–60.

[11] X.C. Jin, S.H. Ong and Jayasooriah, A practical method for estimating fractal dimension, *Pattern Recognition Letters* **16** (1995), 457–464.

[12] J. Markham and J.A. Conchello, Artefacts in restored images due to intensity loss in three-dimensional fluorescence microscopy, *Journal of Microscopy – Oxford* **204** (2001), 93–98.

[13] E.C. Mommers, N. Poulin, C.J. Meijer et al., Malignancy-associated changes in breast tissue detected by image cytometry, *Anal. Cell Pathol.* **20** (2000), 187–195.

[14] L.S. Ploeger, J.A. Belien, N.M. Poulin et al., Confocal 3D DNA cytometry: assessment of required coefficient of variation by computer simulation, *Cell. Oncol.* **26** (2004), 93–99.

[15] J.A. Rice, *Mathematical Statistics and Data Analysis*, 2nd edn, Duxbury Press, Belmont, California, USA, 1995.

[16] M. Schroeder, *Fractals, Chaos and Power Laws*, W.H. Freeman, New York, 1991.

[17] A.M. Snijders, G.A. Meijer, R.H. Brakenhoff et al., Microarray techniques in pathology: tool or toy?, *Mol. Pathol.* **53** (2000), 289–294.

[18] J. Sudbo, S.M. Lippman, J.J. Lee et al., The influence of resection and aneuploidy on mortality in oral leukoplakia, *N. Engl. J. Med.* **350** (2004), 1405–1413.

[19] P. Tekola, J.P. Baak, H.A. van Ginkel et al., Three-dimensional confocal laser scanning DNA ploidy cytometry in thick histological sections, *J. Pathol.* **180** (1996), 214–222.

[20] P.J. van Diest, J. Mouriquand, N.W. Schipper et al., Prognostic value of nucleolar morphometric variables in cytological breast cancer specimens, *J. Clin. Pathol.* **43** (1990), 157–159.

[21] R.W. Veltri, A.W. Partin, J.E. Epstein et al., Quantitative nuclear morphometry, Markovian texture descriptors, and DNA content captured on a CAS-200 Image analysis system, combined with PCNA and HER-2/neu immunohistochemistry for prediction of prostate cancer progression, *J. Cell Biochem. Suppl.* **19** (1994), 249–258.

[22] R.W. Veltri, A.W. Partin and M.C. Miller, Quantitative nuclear grade (QNG): a new image analysis-based biomarker of clinically relevant nuclear structure alterations, *J. Cell Biochem. Suppl.* **35** (2000), 151–157.

[23] S.D. Walter, The partial area under the summary ROC curve, *Stat. Med.* (2005).

[24] D. Zink, A.H. Fischer and J.A. Nickerson, Nuclear structure in cancer cells, *Nat. Rev. Cancer* **4** (2004), 677–687.